Electronic Supplementary Material (ESI) for Nanoscale Horizons.

Electronic Supplementary Information

for

Role of Chemical Interface Damping for Tuning Chemical Enhancement in Resonance Surface-Enhanced Raman Scattering of Plasmonic Gold Nanorods

Min Jung Seo[1], Geun Wan Kim[1], Philippe Vuka Tsalu[1], Seong Woo Moon[1], and Ji Won Ha[1*]

[1]Advanced Nano-Bio-Imaging and Spectroscopy Laboratory, Department of Chemistry, University of Ulsan, 93 Daehak-ro, Nam-gu, Ulsan, South Korea

[*]To whom correspondence should be addressed.

J. W. Ha

Phone: +82-52-712-8012

Fax: +82-52-712-8002

E-mail: jwha77@ulsan.ac.kr

<Table of Contents>

1. Experimental Section

1-1. Materials and Chemicals

Cetyltrimethylammonium bromide (CTAB)-stabilized gold nanorods (AuNRs) (25 nm × 73 nm, 25 nm × 87 nm) were purchased from Nanopartz (Loveland, CO, USA). Probe molecules of cysteamine, *p*-aminothiophenol (*p*-ATP), *p*-mercaptophenol (*p*-MP), thiophenol (TP), *p*-chlorothiophenol (*p*-CTP), *p*-mercaptobenzoic acid (*p*-MBA), *p*-(trifluoromethyl)thiophenol (*p*-TFMTP), and *p*-nitrothiophenol (*p*-NTP) were obtained from Sigma-Aldrich (St. Louis, MO, USA). Ethanol was used as solvent for most of the experiments, and a cysteamine solution was made with 18.2-MΩ pure water. These solution samples were used for Raman measurements.

1-2. Characterization of Gold Nanorods

UV-Vis extinction spectra of AuNR solutions were collected with a Varian Cary 300 UV-Vis spectrophotometer and measured with a micro-scale quartz cell to characterize rare gold nanoparticles and compare the effects of *p*-ATP, *p*-MP, and *p*-NTP probe molecules on AuNRs. These samples were prepared by the same method used for the preparation of SERS samples. A scanning electron microscope (SEM) at 10 kV was used for investigating morphology of AuNRs used in this study with an Si wafer as a substrate.

1-3. Sample Preparation for Single-Particle Spectroscopy

The sample for single-particle spectroscopy was prepared by drop-casting the AuNR solution onto a pre-cleaned glass slide. The concentration of AuNRs drop-cast onto the glass surface was controlled at 1 μm^{-2} to facilitate single-AuNR characterization and to minimize interparticle LSPR coupling. For analysis, a scanning stage was used to position the sample at

the desired location. Therefore, only the scattered light from the selected location was collected by the objective and sent to the entrance of the spectrometer to produce a single-particle spectrum.

1-4. Sample Preparation for Surface-Enhanced Raman Spectroscopy

For SERS sample preparation, a 100-μL aliquot of sample was transferred to a centrifuge tube from the AuNR (25 nm × 87 nm) stock solution and centrifuged at 12,000 rpm for 10 min to remove the CTAB surfactant. The rinsed AuNR sample was resuspended in ethanol, and the probe-molecule solution was added to an appropriate concentration. This colloidal solution was sonicated for a few minutes for adequate dispersion and left at room temperature for approximately 6 h for effective binding. The prepared samples were placed into capillary tubes (wall thickness: 0.25 mm, length: 100 mm). Both ends of the sample capillary tube were sealed to prevent loss of solvent by evaporation.

1-5. Raman Instrumentation

A lab-built Raman spectroscopic system with a 785-nm diode laser was used for all Raman and SERS measurements. The laser power was set to 60 mW; however, the intensity that actually arrived on the stage was half the initial power because of losses along the pathlength. A monochromator with a spectral resolution of 0.1 nm was used with a 600-line/mm grating and a slit width of approximately 100 μm. The Raman spectra were collected using a 40× objective lens with a numerical aperture of 0.75. An Andor CCD camera (Newton Du9209-OE) was used as a detector, and an Andor spectrometer (SHAMROCK 303i, SR-3031-A) transmitted the electric data as a spectrum. All spectra were obtained and analyzed with the Matlab software.

1-6. Real-Time Surface-Enhanced Raman Spectroscopy

For real-time SERS sample preparation, 100 μL of the AuNR solution was transferred to a tube and centrifuged at 2,400 rpm for 30 min to remove the CTAB surfactant. The washed AuNR sample was resuspended in ethanol and sonicated for a few seconds for adequate dispersion. Immediately after the probe-molecule solutions of each concentration were added to the rinsed AuNR solution, the prepared samples were transferred to capillary tubes with 0.25 mm wall thickness and 100 mm length. In real-time experiments, 1 mM *p*-NTP and AuNRs in ethanol were mixed with the sample prepared by SERS methodology. Immediately after the two solutions were mixed, SERS measurements were conducted every 3 min until the Raman signals were saturated. Both ends of the sample capillary tube were sealed to prevent loss of solvent by evaporation.

1-7. Dark-Field Microscopy and Spectroscopy

We used a Nikon inverted microscope (ECLIPSE Ti-U, JAPAN) for dark-field (DF) scattering microscopy. In DF mode, we utilized a Nikon Plan Fluor 100× 0.5–1.3 oil iris objective and a Nikon DF condenser. We used an Andor iXon^{EM}+ CCD camera (iXon Ultra 897, UK) to obtain DF scattering images of the AuNPs. The collected images were analyzed with the Image J software. Furthermore, we obtained DF scattering spectra with an Andor spectrometer (SHAMROCK303i, SR-303I-A, UK) and an Andor CCD camera (NewtonDU920P-OE, UK). For analysis, the scanning stage positioned the sample at the desired location. Thus, only the scattered light from the selected location was collected by the objective. The scattered light was sent to the entrance of the spectrometer, dispersed by a grating (300 lines/mm, center wavelength of 700 nm), and detected by a Newton CCD camera (Andor, UK). The background spectrum was obtained at a region without any particles.

1-8. Correlation Study between SEM and Optical Microscopy

In this study, we correlated SEM images with optical images and spectra of single AuNRs. After cleaning glass slides, a gold pattern was created by evaporating a 5 nm Ti layer followed by a 20 nm Au layer through an indexed copper Transmission Electron Microscopy (TEM) grid (Ted Pella) placed on the cleaned glasses. This pattern aided in locating the same particles in SEM and optical microscopy. First, we took SEM images of single AuNRs well separated on a glass slide. In this correlation study, characterization was carried out using a FEI Quanta ESEM2 SEM operated under low vacuum in a water-vapor atmosphere at 30 kV. We then obtained DF scattering images and spectra of same AuNRs under DF microscopy and spectroscopy.

1-9. Fabrication of a Flow Cell for the CID Studies of Single Gold Nanorods

We fabricated a flow cell using parafilm as a spacer between two coverslips #1 (24 mm × 60 mm). Three channels were cut into the parafilm and six holes were cut into one of the coverslips by using a commercially available CO_2-laser cutter system. The parafilm and coverslips were overlaid so that the holes in one of the coverslips matched with the ends of the channels in the parafilm. The flow cell was placed on a heating plate at 120 °C for a few seconds so that the parafilm melted and the flow cell became airtight.

1-10. Real-Time Thiol Binding Experiments under Dark-Field Spectroscopy

Single particle scattering spectra of Au nanoparticles were obtained at the start of the experiment for reference. Then, an ethanolic 1-mM thiol solution (thiophenols with additional functional groups) was introduced through the flow cell while continuously taking single particle spectra of the same Au nanoparticles (AuNRs) for a period of 60 min. It is important to establish

that a comparable, if not complete, coverage of adsorbed thiol molecules was achieved. The AuNRs were extensively washed with ethanol to make a surface as pristine as possible. Then, thiophenols in ethanol was flowed through the flow cell and the thiol molecules started to adsorb on the AuNR surface. During this process, we recorded the scattering spectra of 20 AuNRs repeatedly for approximately 60 min and extracted the FWHM with respect to the starting value. The LSPR linewidth broadening was determined for each single AAuNR. We found a time evolution typical for a Langmuir adsorption isotherm, i.e., $\theta = 1-\exp(-k_L \cdot c \cdot t)$ where the coverage θ depends on the time t, the thiol concentration c, and the Langmuir adsorption constant k_L. As the thiol concentration was constant to be 1 mM, we simplified the adsorption constant to $k = k_L \cdot c$ and fitted the linewidth broadening due to thiol adsorption with $\Delta\Gamma(t) = \Delta\Gamma_{CID}[1-\exp(-kt)]$. This Langmuir adsorption model yielded the equilibrium value of CID, $\Delta\Gamma_{CID}$, for AuNRs with different thiol samples at complete thiol adsorption.

1-11. Enhancement Factor Calculation in SERS Study[1]

Enhancement factor (EF) indicates the magnitude of signal amplification purely with the following expression. EF is meaningful to compare the enhancement with different conditions of similar experiment.

$$\mathrm{EF} = \frac{I_{\mathrm{SERS}} / N_{\mathrm{SERS}}}{I_{\mathrm{NRS}} / N_{\mathrm{NRS}}} \qquad (8)$$

I_{SERS} : Intensity of SERS signal
N_{SERS} : Number of molecules in SERS
I_{NRS} : Intensity of normal Raman signal
N_{NRS} : Number of molecules in normal Raman

The factors related with intensities (I_{SERS} and I_{NRS}) can be obtained from the SERS and Raman spectrum simply, but the number of molecules in system is hard to know exactly. We assume the samples are homogeneous uniformly and the molecules adsorbed are packed densely with

monolayer. $N_{NRS,}$ number of molecules in normal Raman sample, is estimated ideally with capillary tube and N_{SERS} meaning the number of molecules adsorbed on AuNRs is calculated with the method followed.[2]

$$N_{SERS} = N_d A_{laser} A_N / \sigma \qquad (9)$$

where, N_d indicates the number density of the gold nanoparticles, A_{laser} is the focal spot area of laser, A_N is the footprint area of the gold nanoparticles, and σ means the surface area occupied by a single adsorbed probe molecule. Firstly, to obtain $N_{NRS,}$ the focal laser spot is calculated with the slit width, 100 μm and the capillary tube with the inner diameter of 0.8 mm (Fig. S24). The volume of the capillary tube within the red zone in Fig. S24 regard as the laser spot of 0.05 nm^3. The concentration of sample is 1 mM, and the number of molecules in laser spot can be obtained with Avogadro number, estimated to be about 3.01×10^{13}. For the factor, $N_{SERS,}$ the number of density of gold nanoparticles (N_d) is determined by the concentration of stock solution purchased from Sigma-Aldrich (St. Louis, MO, USA), 6.72×10^{10} /mL, and the total volume of SERS samples is 200 μL, resulting in 3.36×10^{13}/L. The footprint area of the gold nanoparticles (A_N) is estimated with the ideal shape of Fig. S24 determined with SEM images, about 7810 nm^2. Finally, the surface area occupied by an adsorbed probe molecule (σ) is obtained from several references from 0.3 nm^2 to 0.5 nm^2/molecule.[3-5] The intensities of Raman and SERS are collected from the C-S vibration in 1100 cm^{-1} and the C-C ring vibration in 1590 cm^{-1}, respectively, and the calculated EF is shown in Table S2.

2. Supporting Results and Discussion

2-1. Optical Properties of AuNRs at the Single Particle Level

In this study, we used AuNRs for several reasons. First, their unique optical properties are easily controlled by changing their sizes and shapes through well-established synthetic methods. Second, AuNRs with two LSPR modes (transverse and longitudinal) are beneficial for an enhanced optical field due to the lightning effect.[6] In this respect, they are effective SERS substrates in the near-infrared (NIR) region suitable to decrease the effects of Rayleigh scattering.[7] Third, a AuNR has three different facets associated with surface energies, which is favorable for the effective adsorption of molecules onto the surface, forming stable complexes.[8]

The AuNRs used for SERS measurements had an anisotropic shape and unique optical properties that differ from those of gold nanospheres. We first characterized the size distribution of AuNRs by scanning electron microscopy (SEM). Fig. S1A shows an SEM image of AuNRs of anisotropic shape. An additional SEM image showing many AuNRs is provided in Fig. S2. The average length and width of the AuNRs were approximately 86.94 (±5.28) nm and 25.37 (±2.48) nm, respectively (Fig. S3). An extinction spectrum of AuNRs dispersed in water was obtained using a Varian Cary 300 UV–Vis spectrophotometer (Agilent). As shown in Fig. S1B, the UV–Vis extinction spectrum shows two LSPR peaks derived from the shape effect. The peak at 520 nm is a transverse LSPR mode generated by the short axis. The peak at approximately 776 nm in the near-IR region is a longitudinal LSPR mode from the long axis of the AuNRs and is known to be more sensitive.[9, 10]

To better understand the optical properties of the AuNRs used in the present study, we performed a single-particle study under scattering-based dark-field (DF) microscopy and spectroscopy (Fig. S4). The experimental setup for this analysis is provided in Fig. S5. Fig. S6A shows a DF scattering image of single AuNRs with an average size of 86.94 (±5.28) nm × 25.37

(±2.48) nm, yielding an aspect ratio (AR) of ~3.4. Fig. S6B shows single-particle scattering spectra of AuNRs squared in Fig. S6A. The LSPR peak was observed at 763 nm on average, which is consistent with the ensemble spectrum shown in Fig. S1B.

2-2. SERS Measurements at a Resonance Condition

In this study, we used AuNRs with an AR of ~3.4 (Fig. S1A) as SERS substrates and a 785-nm diode laser as an excitation source under a lab-built Raman spectrometer, as shown in Figs. S5 and S7. Notably, the dashed line indicating the 785-nm laser excitation wavelength is very close to the maximum of the longitudinal LSPR peak in Fig. S1B. Therefore, a resonance effect between the longitudinal LSPR peak of the AuNRs and the laser wavelength of 785 nm is expected.[11] The resonance condition for SERS can enable large hot-electron populations to be transferred from AuNRs to probe molecules and favors direct hot-electron transfer (or charge transfer) processes, which are directly correlated with CE in SERS (Fig. S8A).[12] Furthermore, as shown in Fig. S8B, self-assembled monolayer (SAM) probes with thiophenol (TP) molecules with different functional groups at their para-position were used to elucidate the CE mechanism in SERS and its connection with CID in AuNRs. The resonance condition used here has been suggested as theoretically appropriate to investigate the role of CID and its connection to the CE mechanism in SERS, which has yet to be demonstrated experimentally.[13]

In fact, the off-resonance condition has been predominantly used in previous studies to exclude the EM effect, enabling to concentrate on the pure CE. However, we used the resonance condition in this study for two reasons. First, the EM effect has been identified as the primary constituent of enhancement.[12] When the EM effect is weakened by non-resonance conditions, the enhancement effect can be diminished and suffer from poor reproducibility. Even the spontaneous self-assembled monolayer system, which is not an exquisitely designed substrate for extreme enhancements such as our system, may not provide sufficient data for an

effective comparison. To optimize this experiment, we controlled all factors influencing the EM effect and observed a consistent high enhancement of the EM effect while closely observing the CE. Second, the resonance condition can provide a greater enhancement of the Raman signal resulting from the CID effect based on the direct interfacial transfer of plasmon-induced hot electrons generated in metals to adsorbed molecules. The resonance condition used in the present study is therefore a better experimental condition to investigate the role of CID and its connection to the CE mechanism in SERS, which has not been investigated and revealed so far.

2-3. Effects of Chemical Structure of Raman Probes on SERS of AuNRs

Because our probe molecules contain single benzene rings and various electronic substituted groups, as shown in Fig. S9A, we systematically explored the effects of benzene ring conjugation to correlate SERS characteristics to various electronic substituted groups. We first explored the effect of the presence of the conjugation system on SERS, such as an aromatic ring with cysteamine and *p*-ATP, each having identical terminal groups of amine (–NH_2) and thiol (–SH) (Fig. S9A) and linked by a carbon chain or benzene ring, respectively. Because of the similarities of the terminal groups, we can identify and assign the aromatic benzene ring effect in SERS spectra for all of our remaining probes (Fig. S9B). As shown in Figs. S10A and S10B, we compared the normal Raman and SERS spectra of 0.1 M cysteamine and those of 1 mM, 0.1 mM, and 0.01 mM *p*-ATP. As shown in Figs. S10 and S11, even for much higher concentrations of cysteamine, the SERS signal enhancement was weak with respect to *p*-ATP. In addition, the two SERS spectra exhibited very different signatures. For cysteamine, the peaks at 660 cm^{-1} and 740 cm^{-1} have been reported and assigned to the formation of two conformers: *gauche* and *trans* forms, respectively.[6, 14] Indeed, the carbon chain

in cysteamine can flex, in contrast to the *p*-ATP rigid benzene ring, which enables another interaction between Au and amine through bending. Of the two conformers, the *trans* form binds to the thiol group only, whereas both functional groups can interact with a Au surface in the *gauche* conformer, suggesting that the *gauche* form provided greater enhancement potential because of the strong interaction with AuNR surfaces. However, the unexpectedly stronger signals (or enhancement) of *p*-ATP can only be explained by the difference between molecular structures,[15] not only the resonance hybrid benzene ring, but also the substitution effects. A benzene ring has planar delocalized π-electrons, whereas cysteamine carbon chains have restricted *σ*-bonding. Thus, the six carbons in a benzene ring can share electrons equally, facilitating fast and active electron flow. Therefore, *p*-ATP with an aromatic benzene ring results in higher SERS enhancement and the benzene ring can successfully amplify Raman signals because of its structural properties.

3. Supporting Figs.

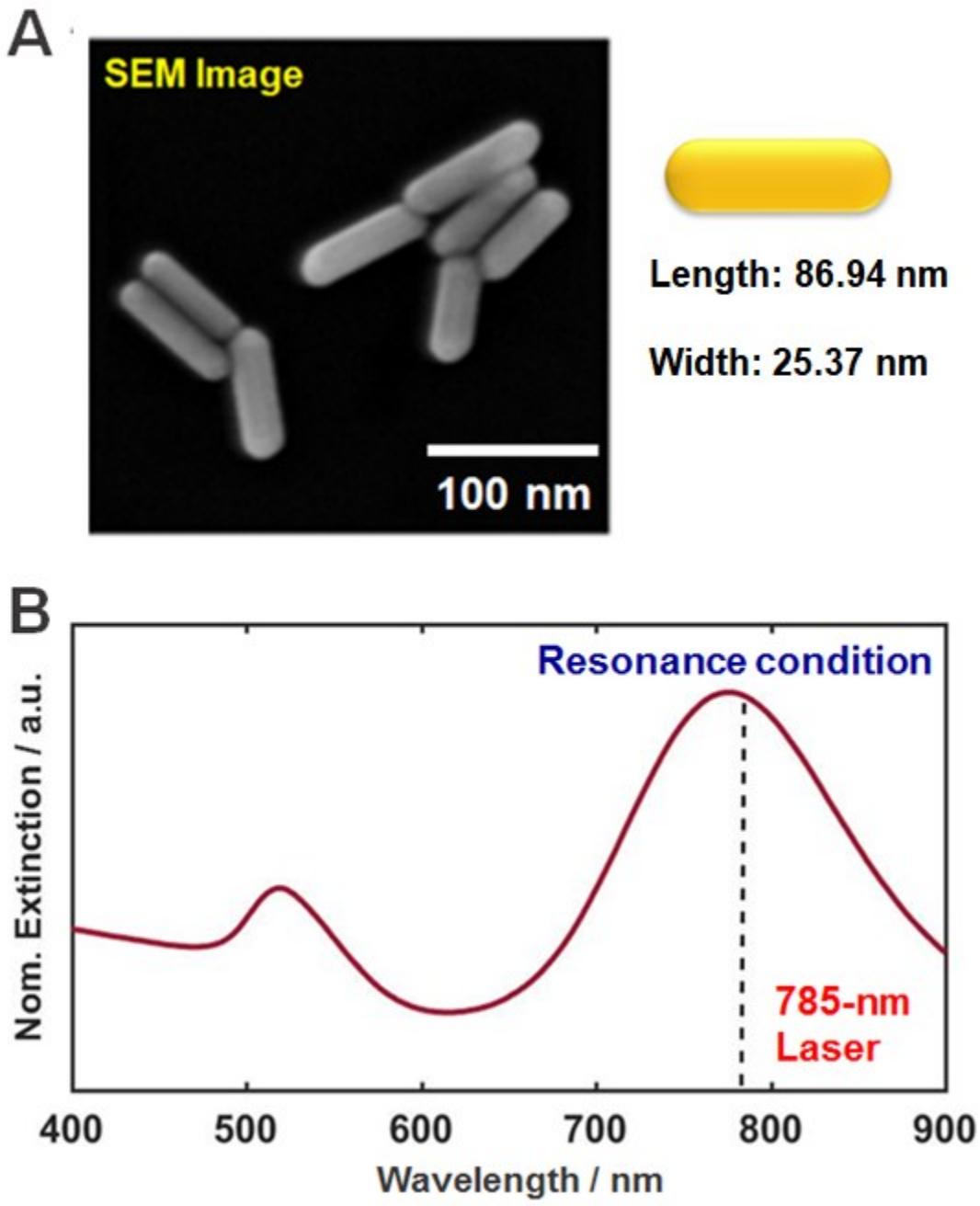

Fig. S1 (A) SEM image of AuNRs and a model of AuNRs with the average size of 25.37 nm × 86.94 nm. **(B)** UV–Vis extinction spectrum of AuNRs showing two distinct LSPR peaks; the dotted-line indicates the resonance condition with a 785-nm Raman laser.

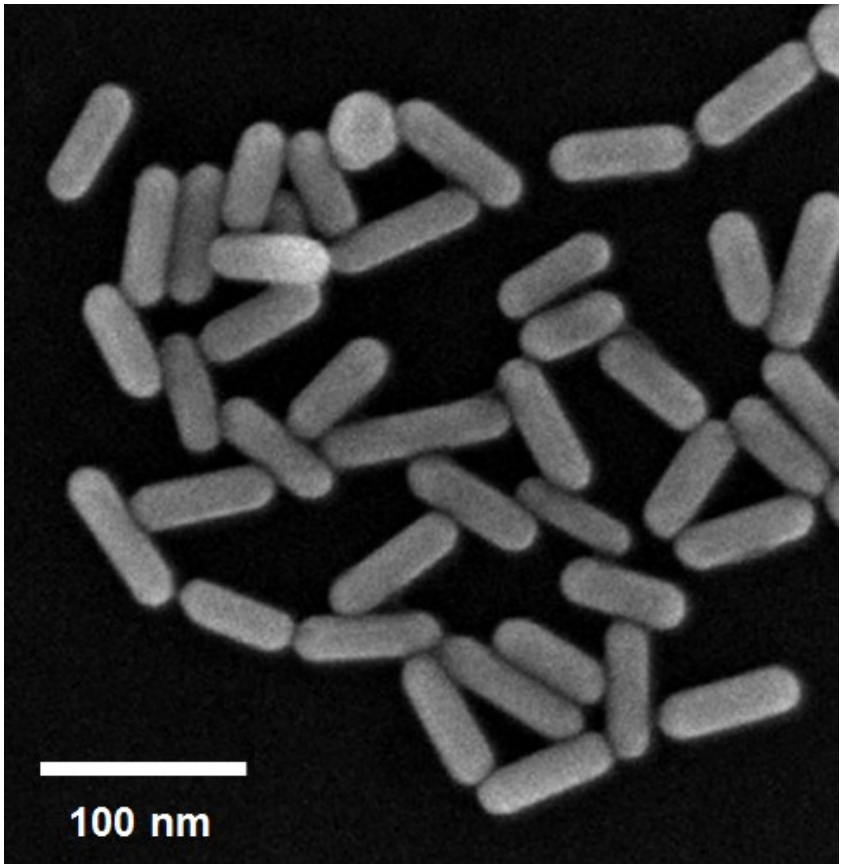

Fig. S2 SEM image of AuNRs (25 nm × 87 nm) used in this Raman study.

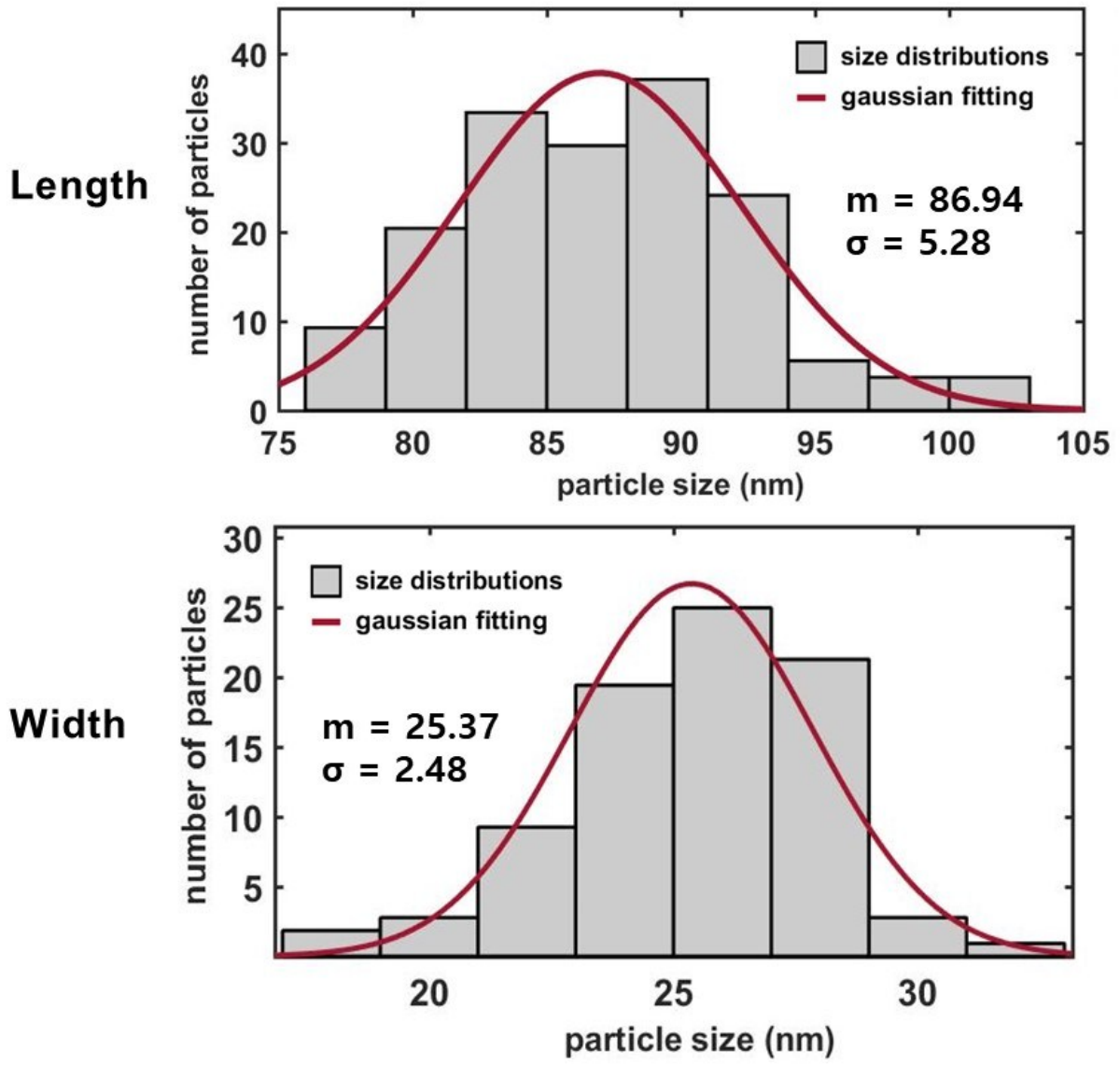

Fig. S3 Size distributions of AuNRs with gaussian fitting. The average length and width were determined to be 86.94 nm and 25.37 nm, respectively. Total 90 particles were counted from SEM images to build the histrograms.

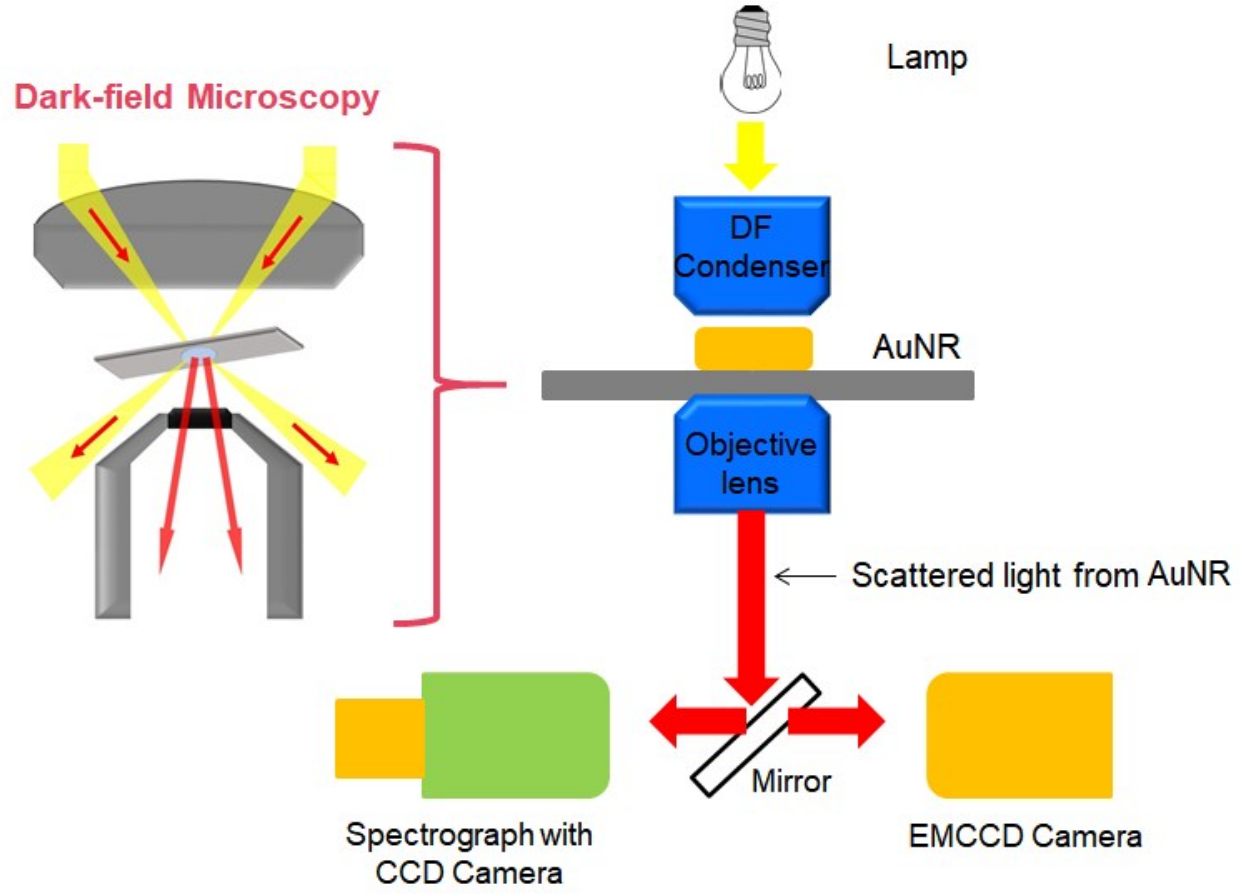

Fig. S4 A schematic to depict the working principle of DF microscopy and spectroscopy. The blue-arrow indicates the direction of light from lamp. Only scattered light from the sample (red-color) is directed either to a spectrograph (left) or to a EMCCD camera (right).

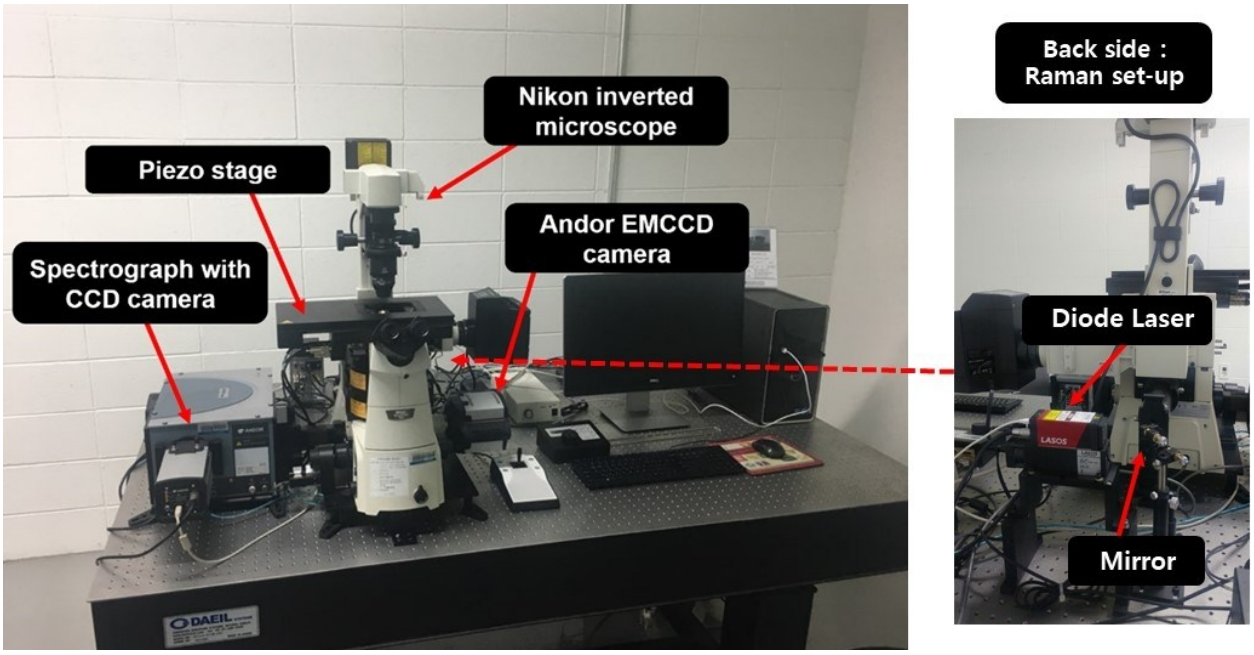

Fig. S5 A photograph showing the experimental setup for Raman spectroscopy and DF single particle scattering spectroscopy. The back side shows the laser source and beam paths for Raman measurement.

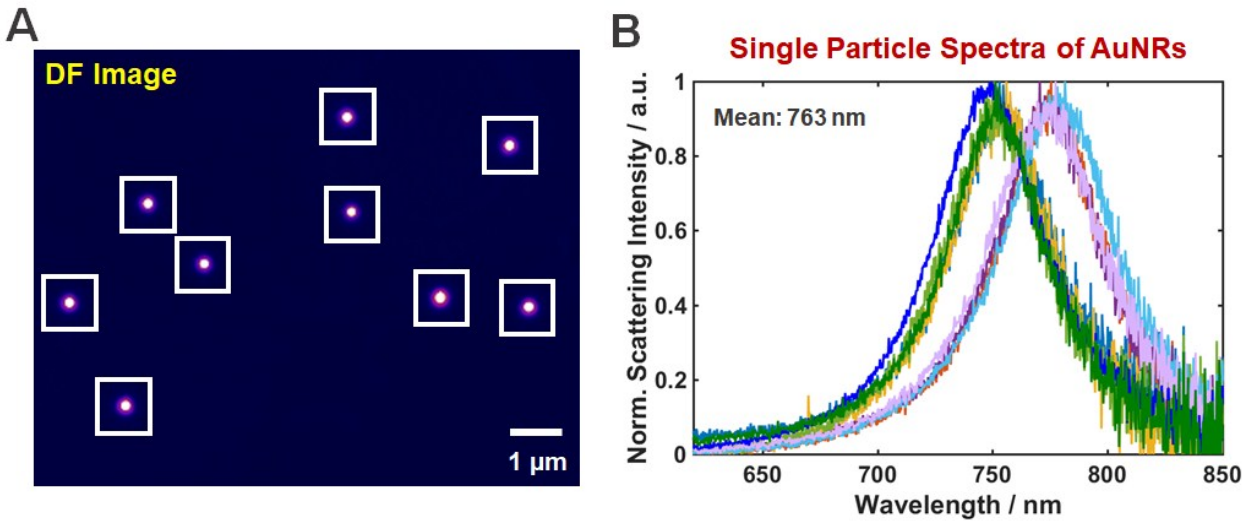

Fig. S6 (A) DF scattering image of single AuNRs (25.4 nm × 86.9 nm on average). **(B)** Single particle scattering spectra of of AuNRs squared in (A). The mean longitudinal LSPR wavelength of the AuNRs is 763 nm.

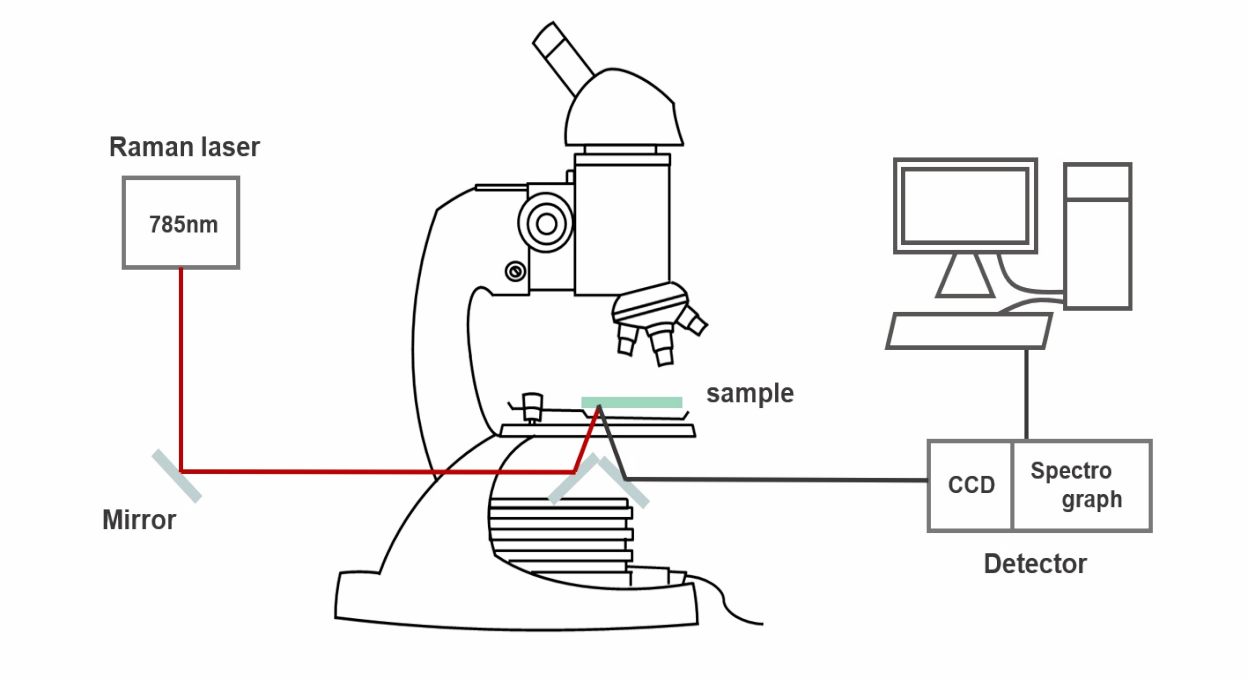

Fig. S7 A schematic depicting the experimental setup of a home-built Raman spectroscope with a 785-nm diode laser.

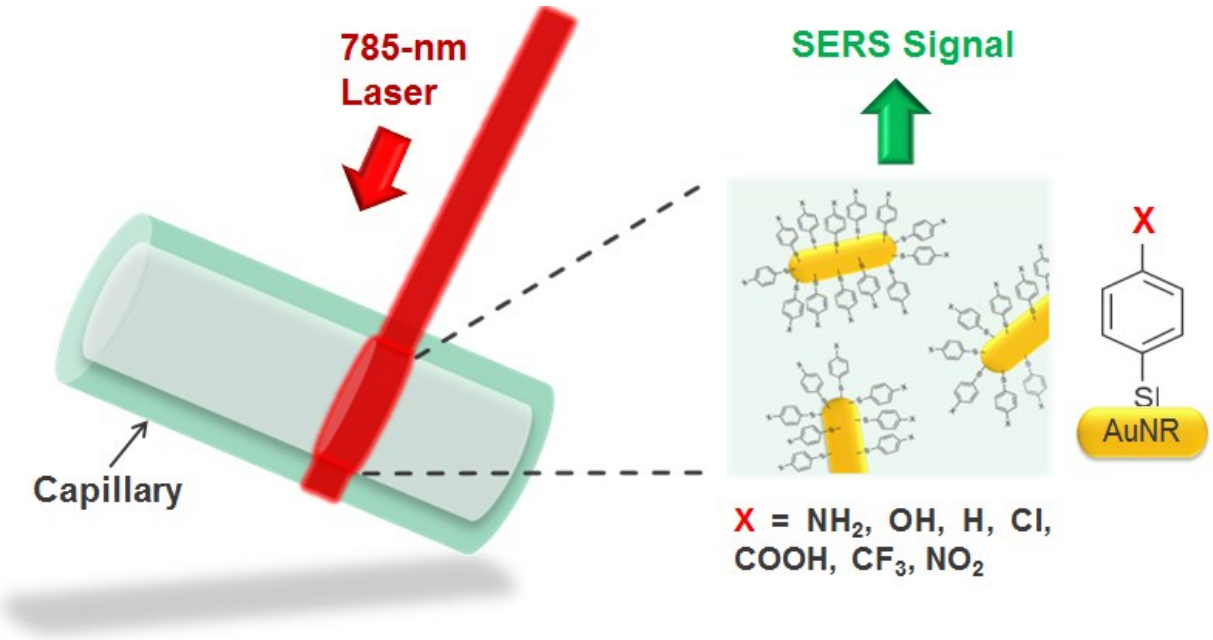

Fig. S8 Schematic of SERS measurement with capillary tube and self-assembled monolayer (SAM) systems.

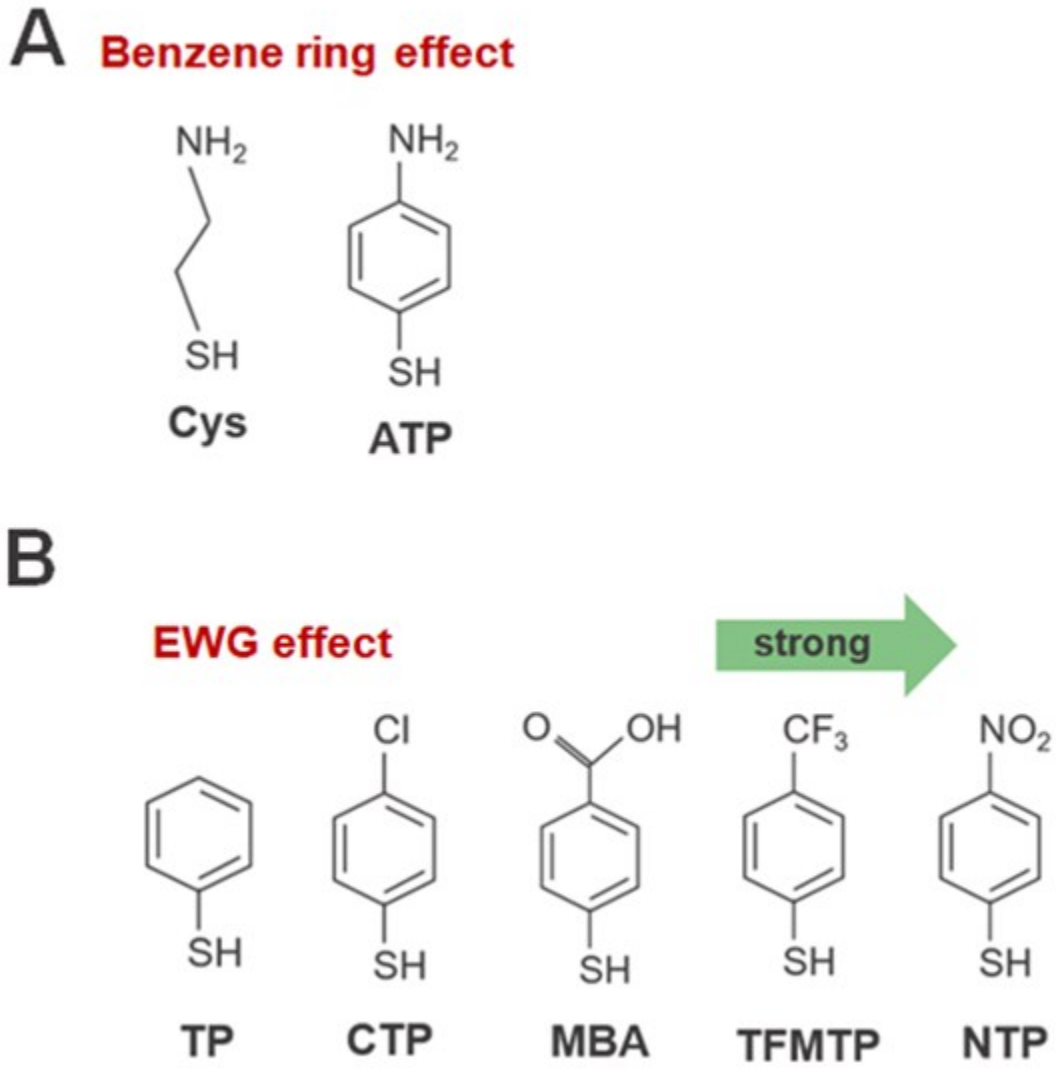

Fig. S9 Classified probe molecules used in this study. **(A)** Cysteamine and *p*-ATP (*p*-aminothiophenol) for benzene ring effect, **(B)** TP (thiophenol) as a standard and *p*-CTP (*p*-chlorothiophenol), *p*-MBA (*p*-mercaptobenzoic acid), *p*-TFMTP (p-trifluoromethylthiophenol), and *p*-NTP (p-nitrothiophenol) for studying the EWG effect.

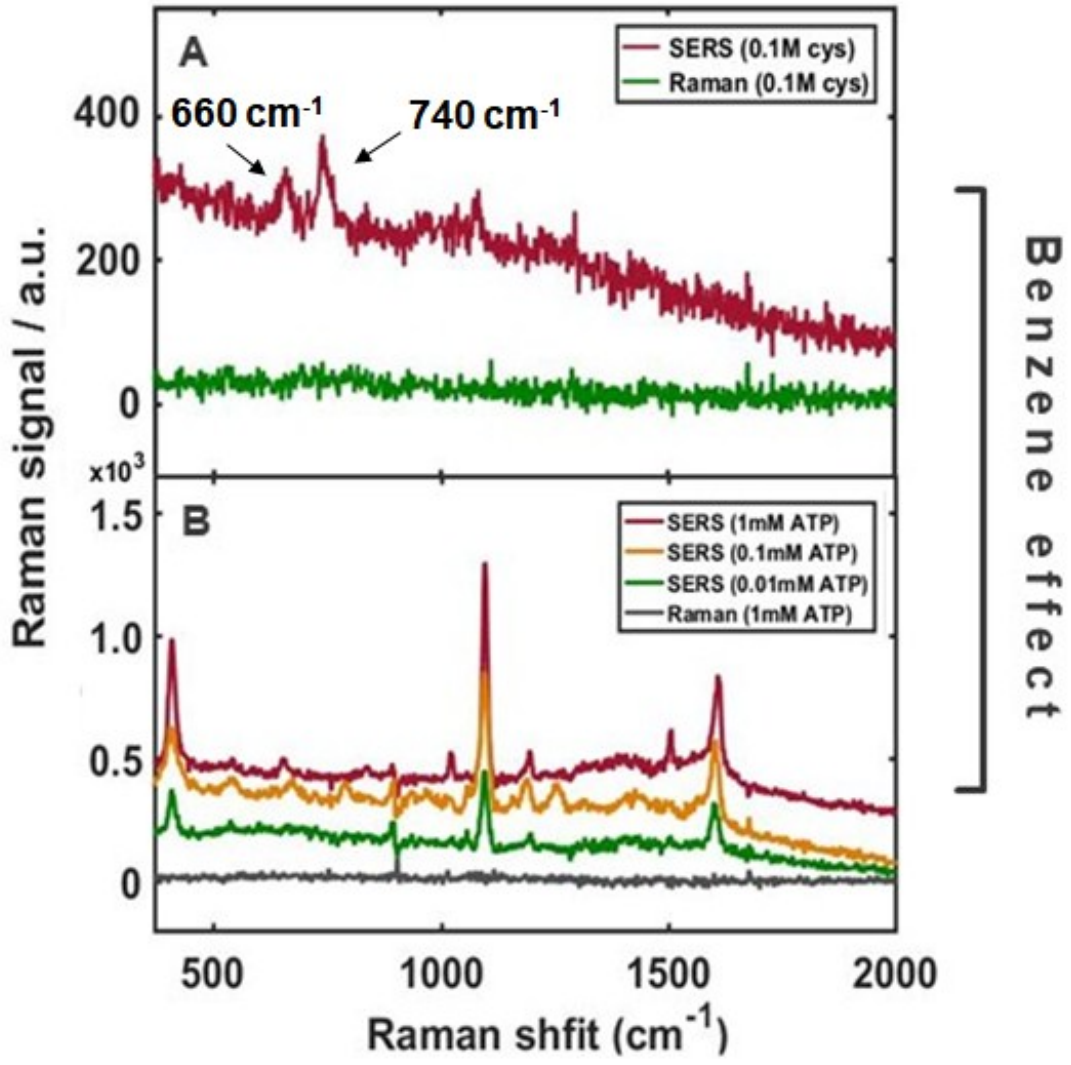

Fig. S10 SERS and Raman spectra of **(A)** cysteamine and **(B)** *p*-ATP for studying the effect of benzene ring.

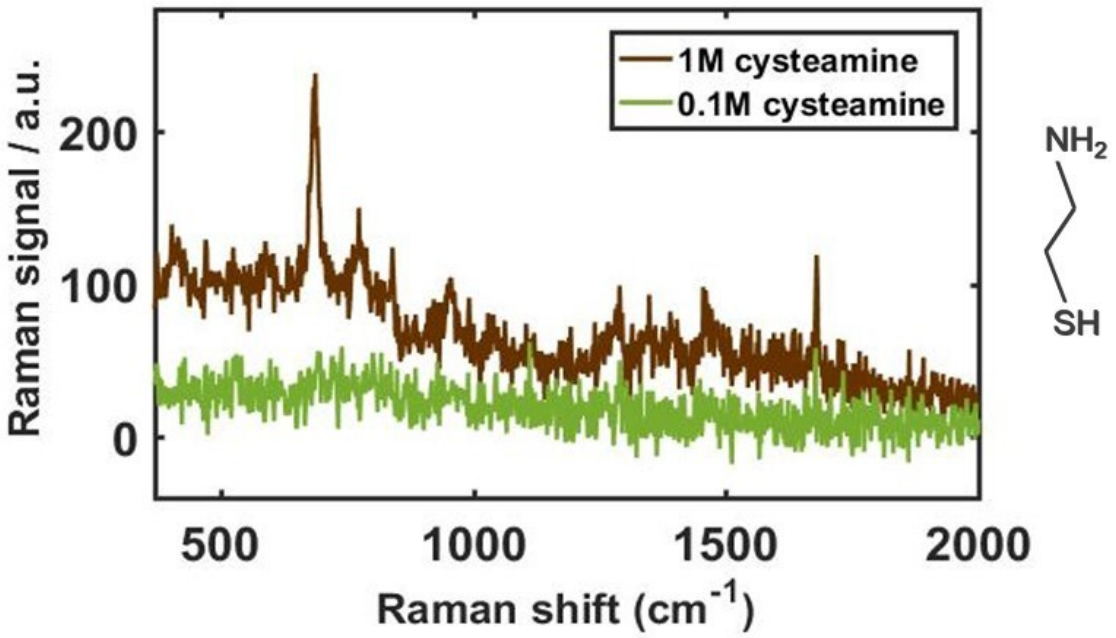

Fig. S11 Raman spectra of Cysteamine in solution at the concentrations of 0.1 M and 1M.

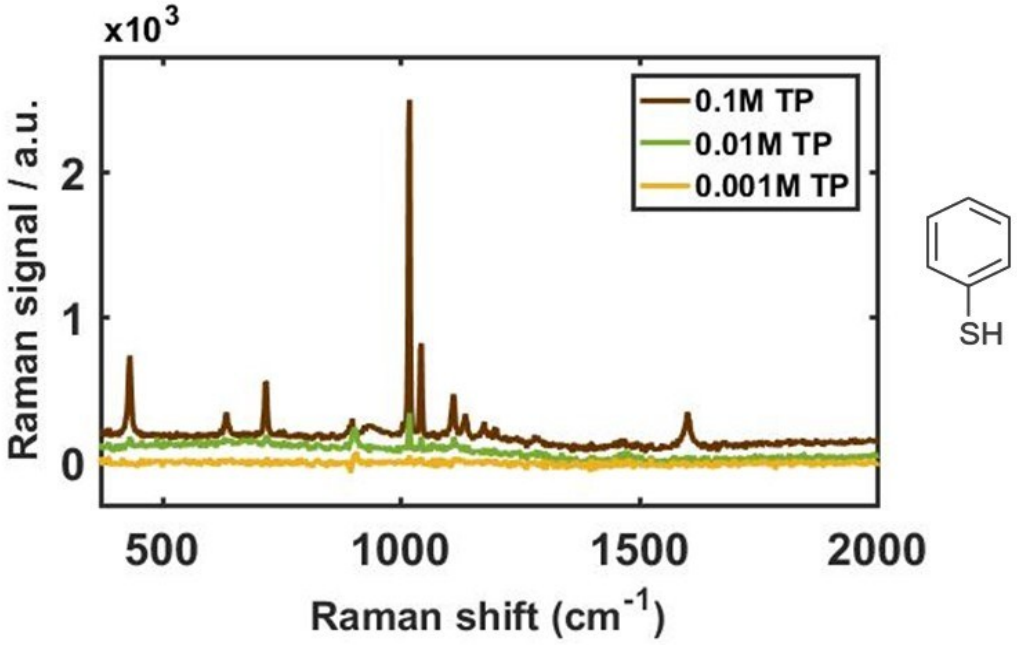

Fig. S12 Raman spectra of thiophenol (TP) at diverse concentrations

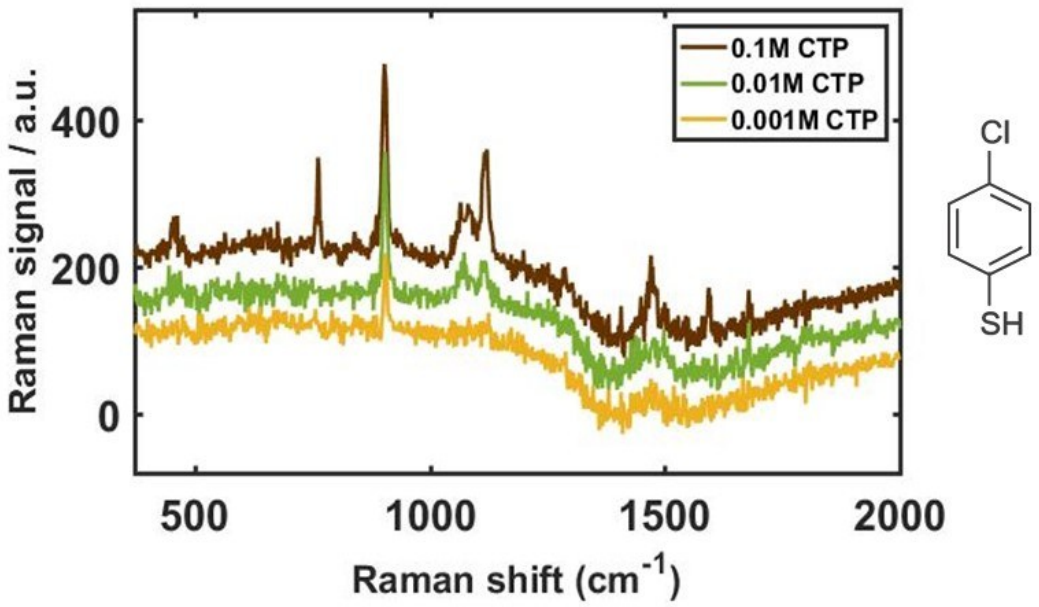

Fig. S13 Raman spectra of *p*-chlorothiophenol (*p*-CTP) at diverse concentrations

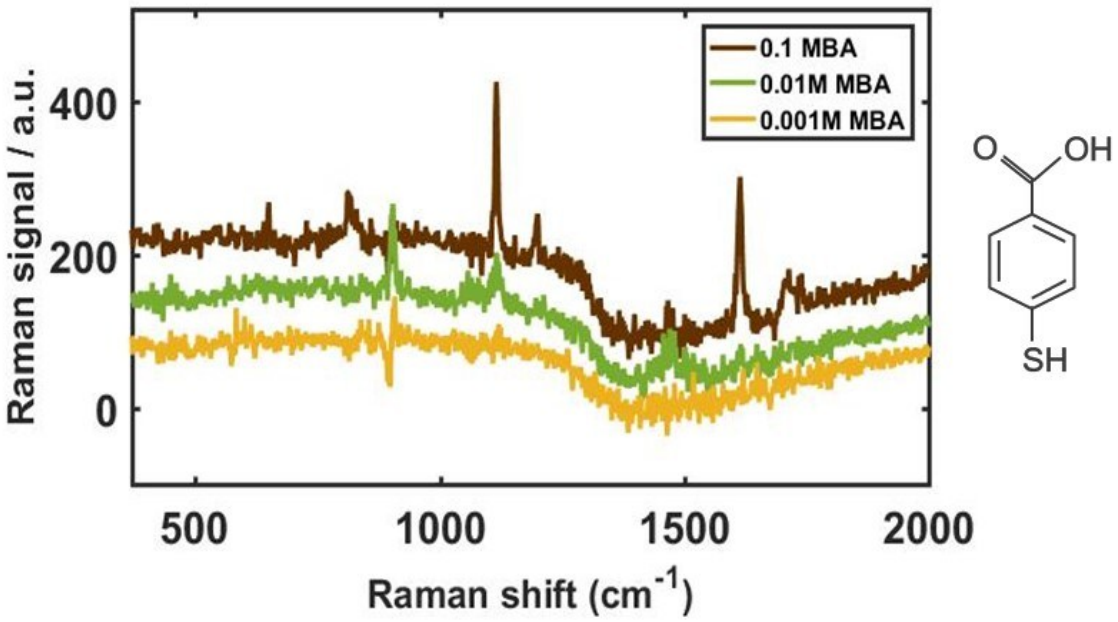

Fig. S14 Raman spectra of *p*- mercaptobenzoic acid (*p*-MBA) at diverse concentrations

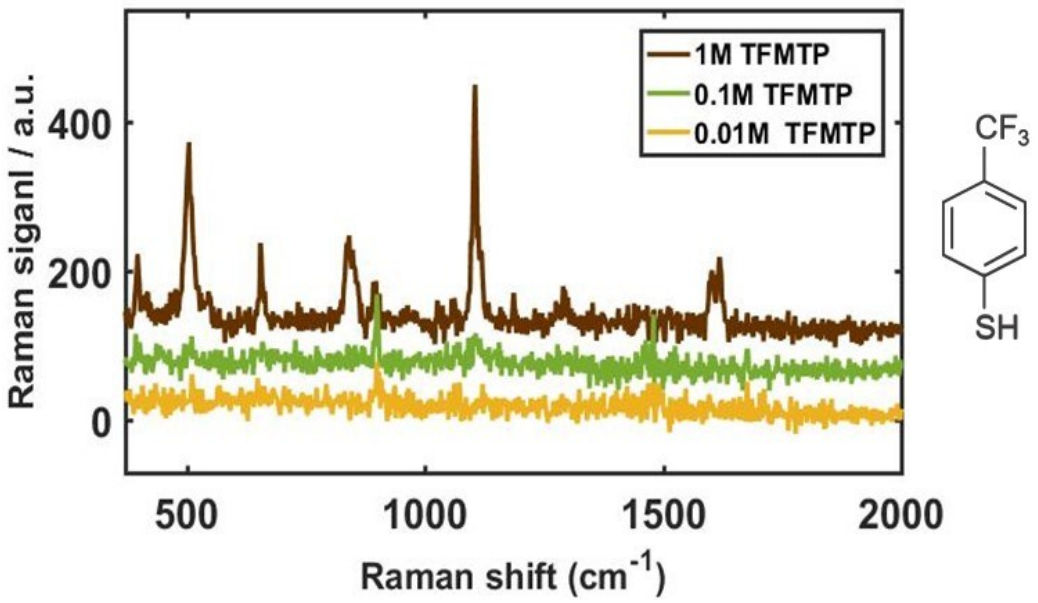

Fig. S15 Raman spectra of *p*-trifluoromethyl thiophenol (*p*-TFMTP) at diverse concentrations

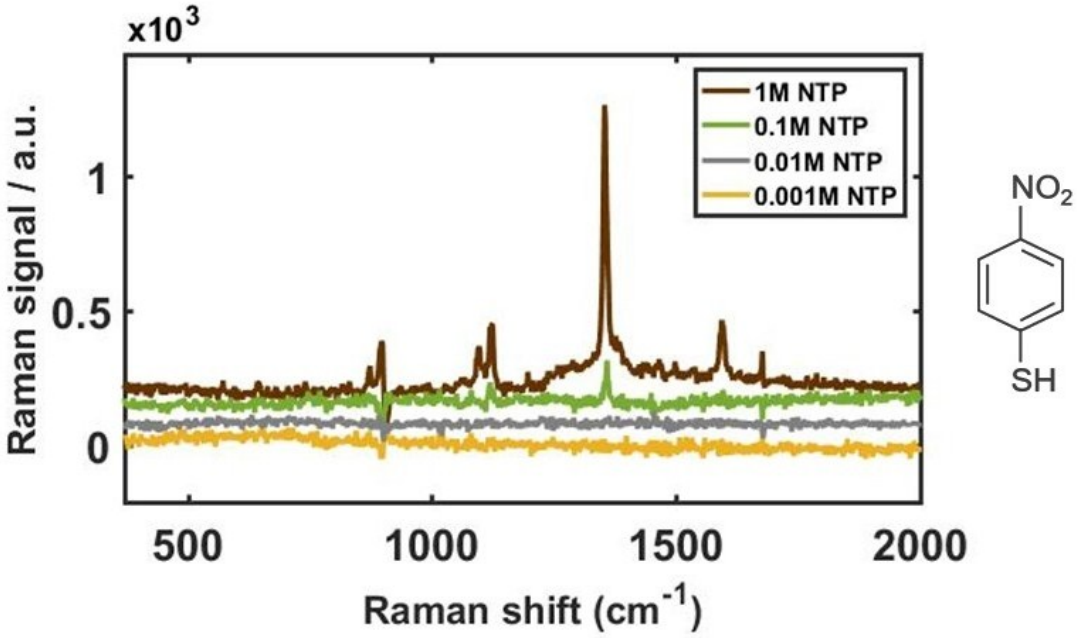

Fig. S16 Raman spectra of *p*- nitrothiophenol (*p*-NTP) at diverse concentrations

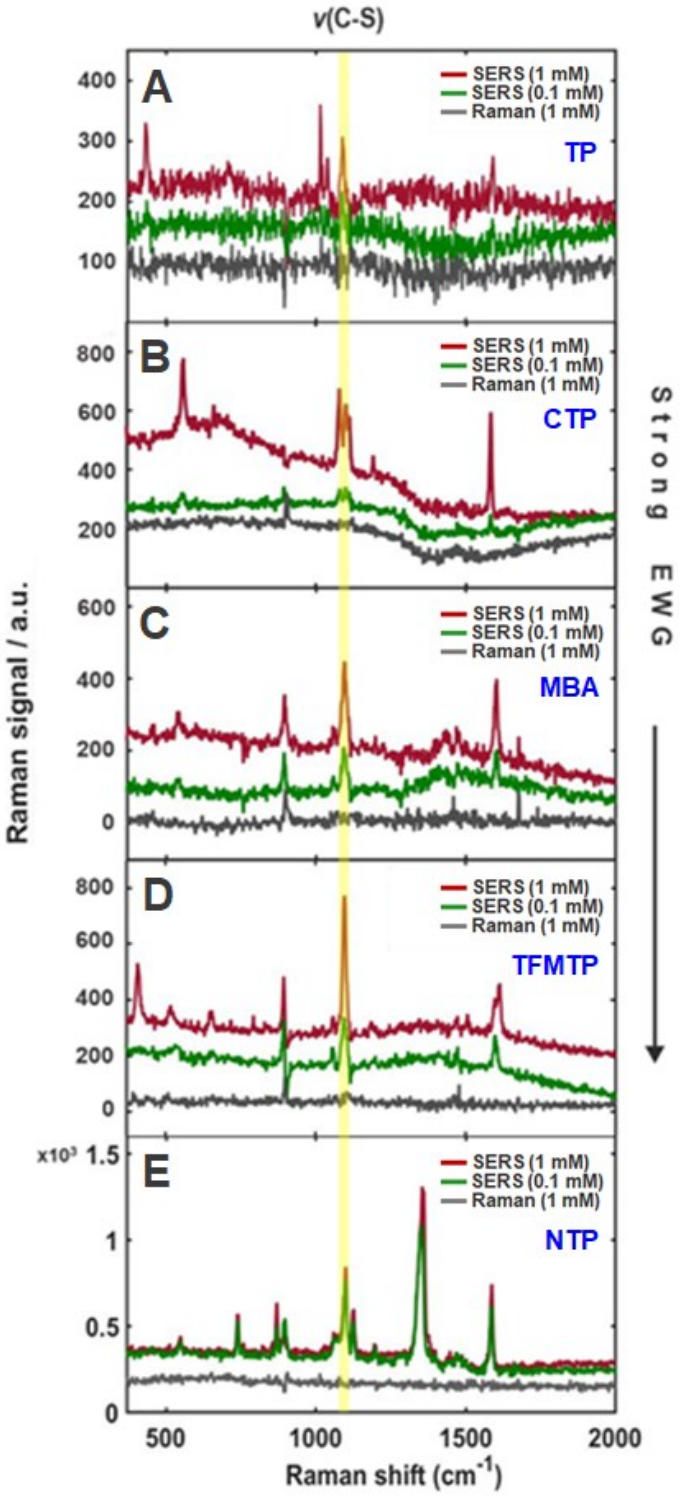

Fig. S17 Complete SERS spectra for all of the electron withdrawing groups (EWGs) used in this study.

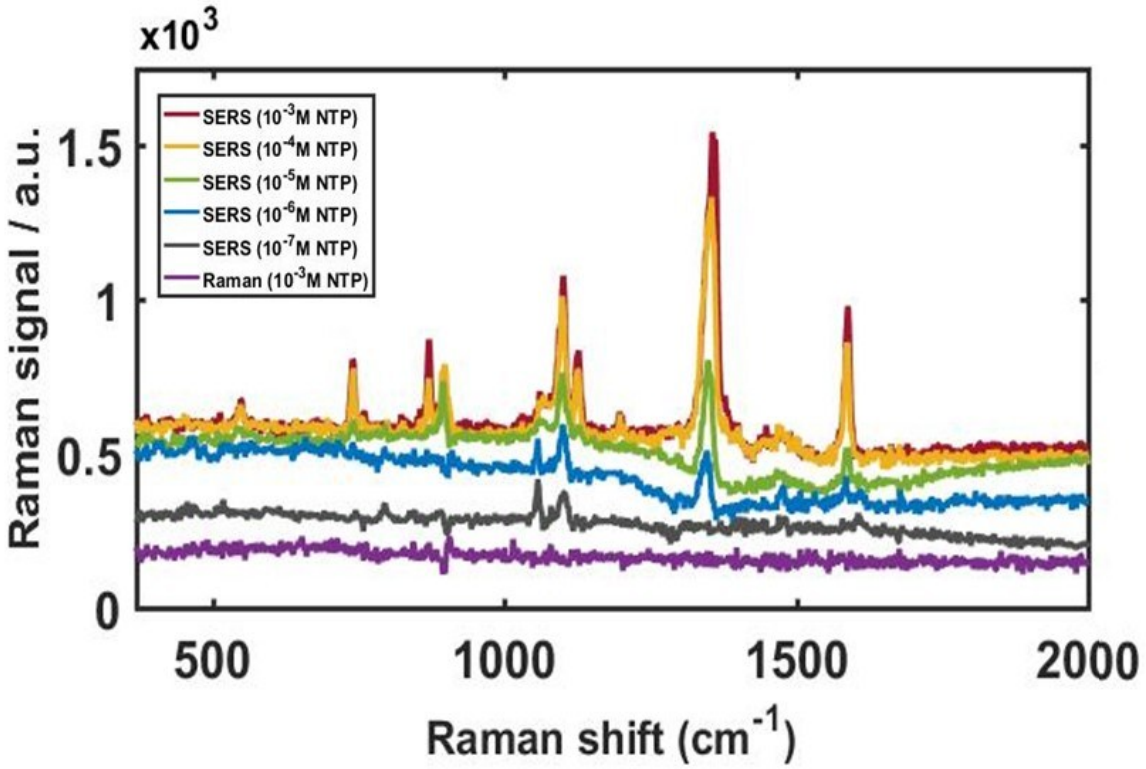

Fig. S18 SERS spectra of *p*-NTP at diverse concentrations. The lowest concentration was 100 nM.

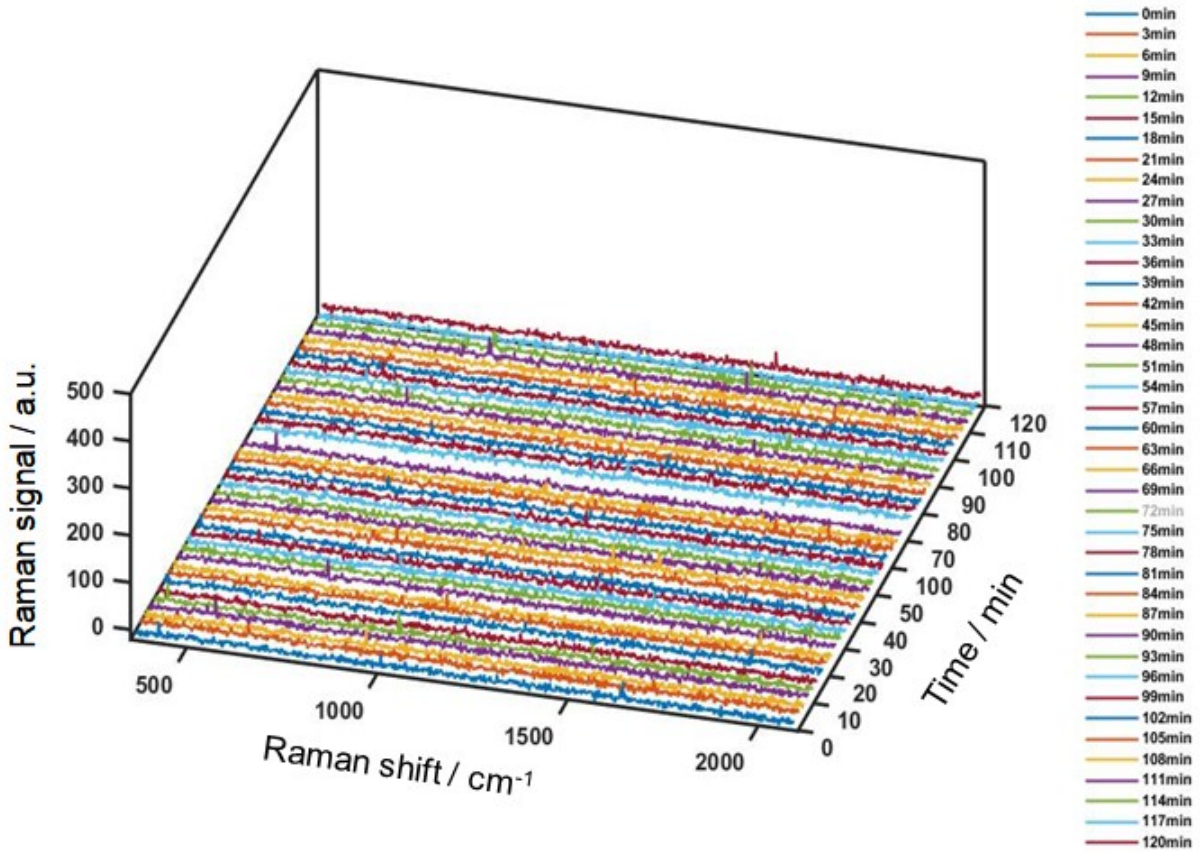

Fig. S19 Control experiment. Raman spectra of *p*-NTP in the absence of AuNRs in solution.

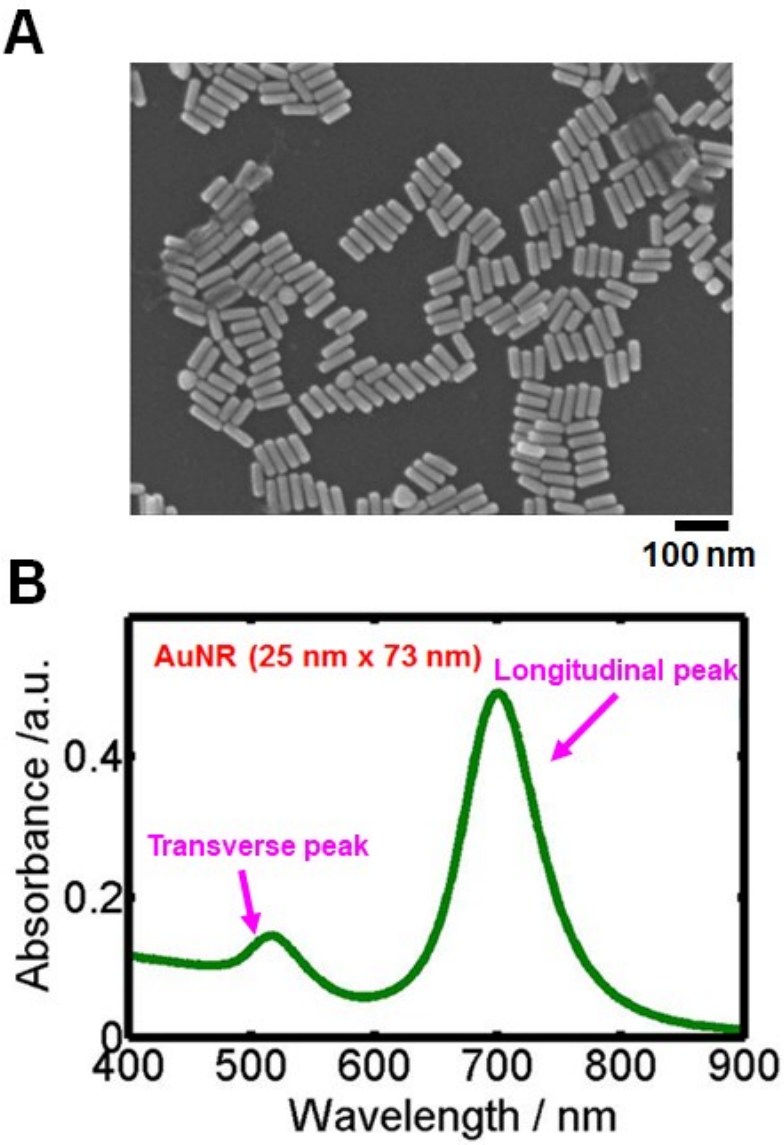

Fig. S20 (A) SEM image of AuNRs (25 nm × 73 nm, on average) used for CID experiments. **(B)** UV-Vis absorption spectrum of AuNRs showing two typical LSPR peaks. The longitudinal LSPR peak appears at approximately 716 nm.

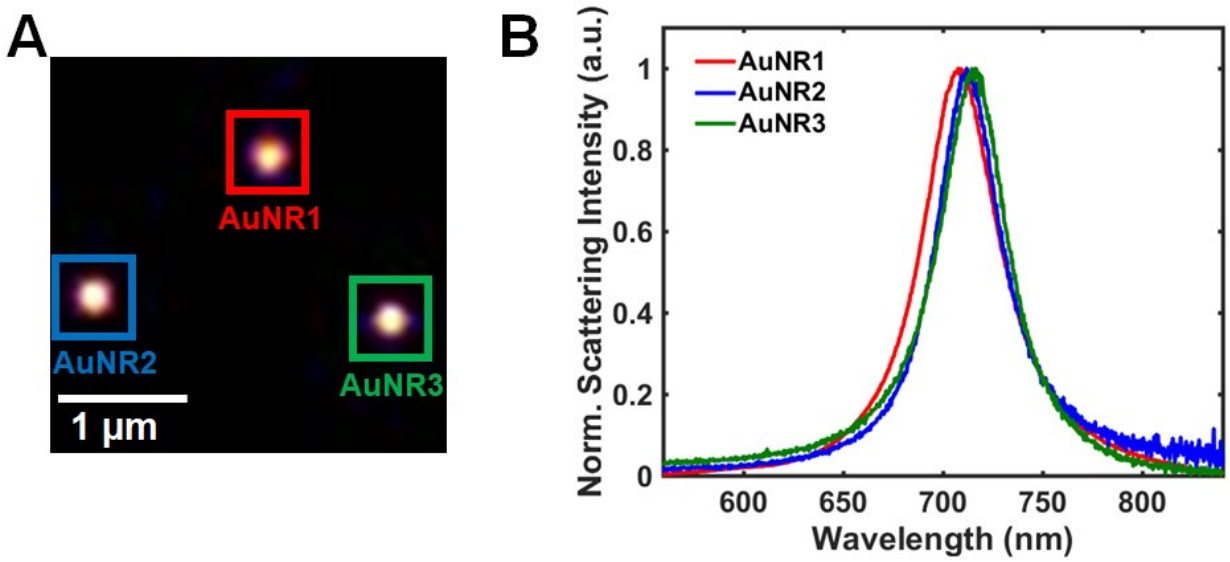

Fig. S21 (A) DF scatterig image of single AuNRs (25 nm × 73 nm). **(B)** Single particle scattering spectra of three AuNRs highlighted with a square in (A).

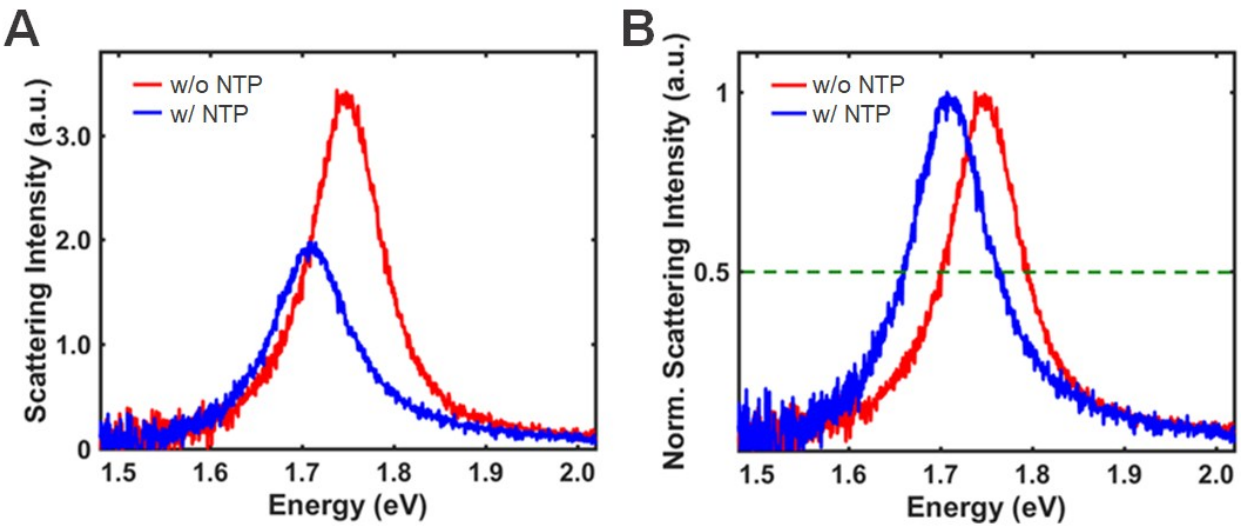

Fig. S22 (A) Single particle scattering spectra of a AuNR (25 nm × 73 nm) without *p*-NTP and 30 min after the adsorption of *p*-NTP on the AuNR surface. **(B)** The broadening of LSPR linewidth is better illustrated in the normalized scattering spectra.

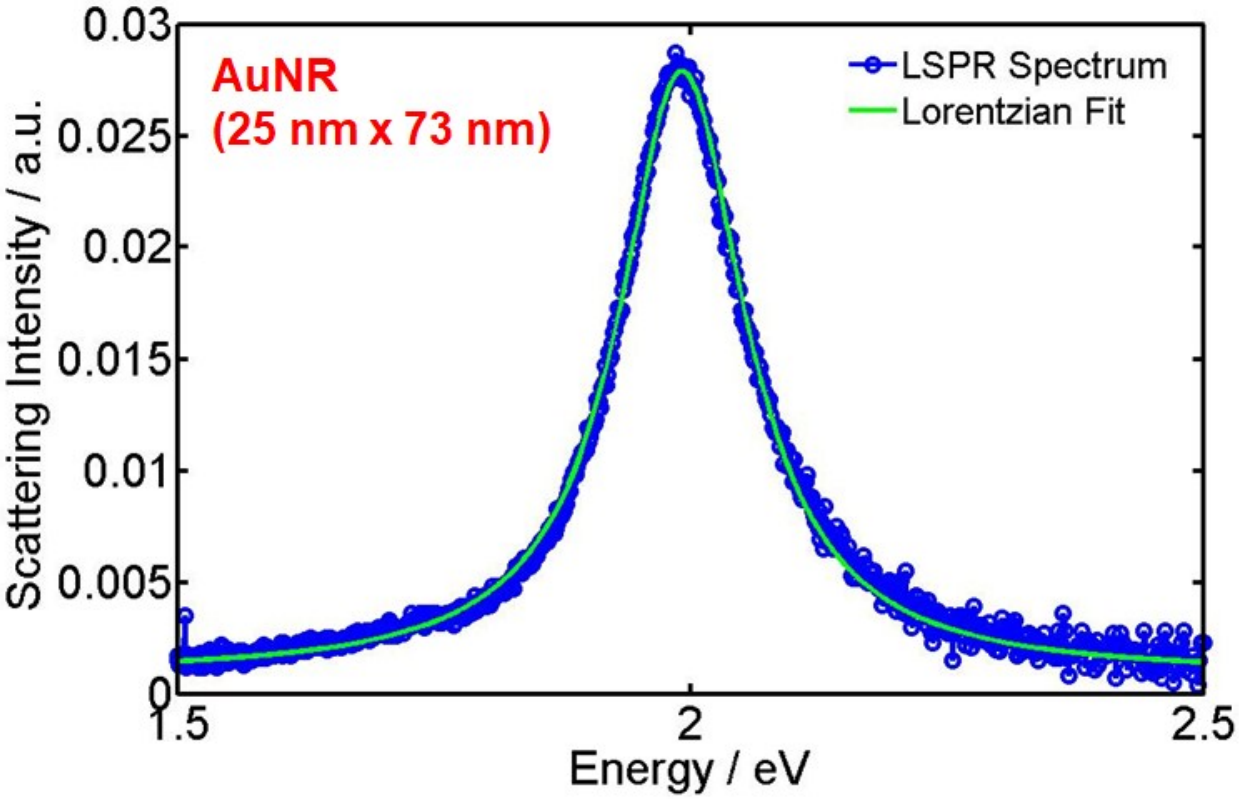

Fig. S23 The single particle spectrum of a AuNR (25 nm × 73 nm) is fitted with Lorentzian function (green-curve) to yield the LSPR linewidth and resonant frequency.

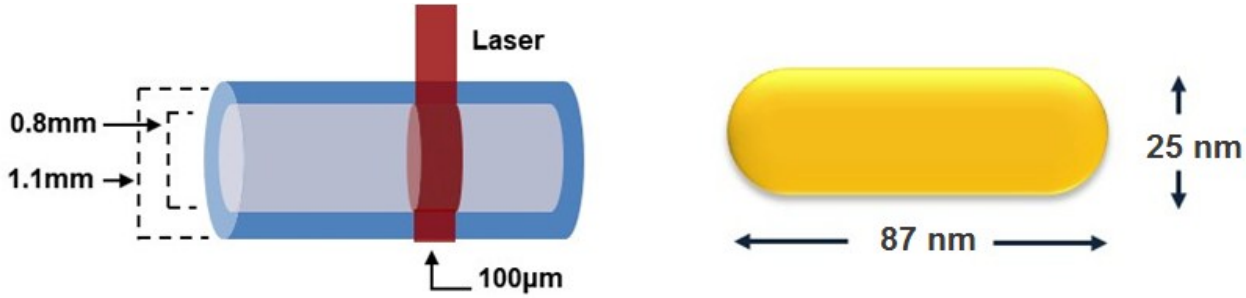

Fig. S24 The ideal model of the focal spot of laser and surface area of a AuNR for calculating EF factors.

4. Supporting Table

Probe molecule	Raman (solid)	Raman (solution)	SERS	Vibrational assignment
cysteamine		688	660	$\nu(C\text{-}S)_G$; gauche
	777	774	740	$\nu(C\text{-}S)_T$; trans
	1031	1040	1075	ν(C-C-N)
p-ATP	385	396	407	δ(C-S)
	1088	1108	1096	*ν*(C-S)
	1180	1197	1195	δ(C-H)
	1497	1515	1507	*ν*(C-C) + δ(C-H)
	1596	1616	1609	*ν*(C-C)
p-MP		798	796	π(C-H)
			895	ɣ(C-H)
		1122	1100	*ν*(C-S) + *ν*(C-H) + *ν*(C-C)
		1628	1611	*ν*(C-C)
TP		432	431	*ν*(C-H)
		1019	1015	*ν*(C-C), δ(C-H)
		1110	1089	*ν*(C-S)
		1601	1592	*ν*(ring)
p-CTP			560	*ν*(C-Cl)
		1072	1080	*ν*(C-C), *ν*(C-S)
	1115	1115	1103	δ(C-H)
	1611	1594	1586	*ν*(C-C)
p-MBA	931	904	896	δ(C-O-O)
	1119	1115	1096	*ν*(C-S)
	1590	1614	1605	*ν*(C-C)
p-TFMTP		396	407	*ν*(C-F)
		1105	1098	*ν*(C-S)
		1603	1600	*ν*(C-C)
p-NTP	873	873	871	π(C-H)
	1096	1096	1100	*ν*(C-S)
	1117	1122	1126	*ν*(C-N)
	1348	1353	1357	$\nu(NO_2)$
	1592	1594	1589	*ν*(C-C)

Table S1. Raman and SERS peak assignments for each probe molecule, obtained from Refs.[14-26] (ν : vibration, δ, ɣ : bending, π : wagging)

Probe molecule	EF (C-S)	EF (C-C_{ring})
ThioPhenol	3.33×10^4	1.87×10^4
ChloroThioPhenol	2.06×10^5	2.07×10^5
MercaptoBenzoic Acid	1.41×10^5	2.11×10^5
TriFluoroMethylThioPhenol	1.75×10^6	2.35×10^6
NitroThioPhenol	3.33×10^6	3.31×10^6

Table S2. Calculated ehnancement factors for EWGs at the C–S vibration of 1100 cm^{-1} and the C–C vibration of 1590 cm^{-1}.

5. Supporting References

1. H. Jia, X. Bai, N. Li, L. Yu and L. Zheng, *CrystEngComm*, 2011, **13**, 6179-6184.
2. C. J. Orendorff, L. Gearheart, N. R. Jana and C. J. Murphy, *Physical Chemistry Chemical Physics*, 2006, **8**, 165-170.
3. J. Huang, Y. Zhu, M. Lin, Q. Wang, L. Zhao, Y. Yang, K. X. Yao and Y. Han, *Journal of the American Chemical Society*, 2013, **135**, 8552-8561.
4. S. Sergiienko, K. Moor, K. Gudun, Z. Yelemessova and R. Bukasov, *Physical Chemistry Chemical Physics*, 2017, **19**, 4478-4487.
5. P. N. Sisco and C. J. Murphy, *The Journal of Physical Chemistry A*, 2009, **113**, 3973-3978.
6. J. Aizpurua, G. W. Bryant, L. J. Richter, F. G. De Abajo, B. K. Kelley and T. Mallouk, *Physical Review B*, 2005, **71**, 235420.
7. M. Suzuki, Y. Niidome, N. Terasaki, K. Inoue, Y. Kuwahara and S. Yamada, *Japanese journal of applied physics*, 2004, **43**, L554.
8. Z. Wang, M. Mohamed, S. Link and M. El-Sayed, *Surface Science*, 1999, **440**, L809-L814.
9. P. Zijlstra, J. W. Chon and M. Gu, *nature*, 2009, **459**, 410.
10. E. T. Castellana, R. C. Gamez, M. E. Gómez and D. H. Russell, *Langmuir*, 2010, **26**, 6066-6070.
11. H. Zhang, S. Yang, Q. Zhou, L. Yang, P. Wang and Y. Fang, *Plasmonics*, 2017, **12**, 77-81.
12. A. Campion and P. Kambhampati, *Chemical society reviews*, 1998, **27**, 241-250.
13. F. Hubenthal, *Applied Physics B*, 2014, **117**, 1-5.

14. S. Bloxham, O. Eicher-Lorka, R. Jakubėnas and G. Niaura, *Spectroscopy letters*, 2003, **36**, 211-226.

15. A. Kudelski and W. Hill, *Langmuir*, 1999, **15**, 3162-3168.

16. M. Abdelsalam, *Open Chemistry*, 2009, **7**, 446-453.

17. R. Holze, *Physical Chemistry Chemical Physics*, 2015, **17**, 21364-21372.

18. X. Hu, T. Wang, L. Wang and S. Dong, *The Journal of Physical Chemistry C*, 2007, **111**, 6962-6969.

19. R. Li, W. Ji, L. Chen, H. Lv, J. Cheng and B. Zhao, *Spectrochimica Acta Part A: Molecular and Biomolecular Spectroscopy*, 2014, **122**, 698-703.

20. R. Li, H. Lv, X. Zhang, P. Liu, L. Chen, J. Cheng and B. Zhao, *Spectrochimica Acta Part A: Molecular and Biomolecular Spectroscopy*, 2015, **148**, 369-374.

21. S. Mahajan, T. Hutter, U. Steiner and P. Goldberg Oppenheimer, *The Journal of Physical Chemistry Letters*, 2013, **4**, 4153-4159.

22. B. L. Scott and K. T. Carron, *The Journal of Physical Chemistry C*, 2016, **120**, 20905-20913.

23. C. E. Taylor, J. E. Pemberton, G. G. Goodman and M. H. Schoenfisch, *Applied spectroscopy*, 1999, **53**, 1212-1221.

24. P. Wang, H. Li, C. Cui and J. Jiang, *Applied Surface Science*, 2017, **425**, 833-837.

25. Y. S. Yamamoto, Y. Kayano, Y. Ozaki, Z. Zhang, T. Kozu, T. Itoh and S. Nakanishi, *arXiv preprint arXiv:1610.08270*, 2016.

26. X. Zhang, Z. Yu, W. Ji, H. Sui, Q. Cong, X. Wang and B. Zhao, *The Journal of Physical Chemistry C*, 2015, **119**, 22439-22444.